Available online at www.sciencedirect.com
ScienceDirect
Ceramics International 36 (2010) 1645–1651
CERAMICS INTERNATIONAL
www.elsevier.com/locate/ceramint

In vitro bioactivity of novel cured ionomer cement based on iron oxide

Jhamak Nourmohammadi *, S.K. Sadrnezhaad, A. Behnamghader

Biomaterials Department, Material and Energy Research Center, P.O. Box 14155-4777, Tehran, Iran

Received 6 July 2009; received in revised form 21 January 2010; accepted 20 February 2010
Available online 25 March 2010

Abstract

The effect of adding Fe_2O_3 on the bioactivity of cured ionomer cement was examined in simulated body fluid (SBF). Although the polyacrylic acid and Fe_2O_3 are known as inhibitors for apatite formation, results clearly show that exposure of the cement to the SBF lead to the formation of rough layers of carbonated-apatite (Volmer–Weber growth). Interestingly, the addition of Fe_2O_3 to the cement structure decreases the possibility of acid–base reaction in ionomer cements due to the improved chemical durability of the glass. Therefore, more calcium ions were released from the cement at the initial stage of soaking which plays an important role in forming the surface apatite layer by heterogeneous nucleation via the OH^- groups on the cement surface.

Keywords: Resin-modified glass-ionomer cement; Iron oxide; Carbonated-apatite; Simulated body fluid; Bone cement

1. Introduction

Polymethylmethacrylate (PMMA) has been widely used as bone cement. However, it does not show any bioactivity and hence its fixation is liable to degrade over a long time [1]. Accordingly, extensive attempts have been made to obtain bioactive cement with suitable properties. Glass-ionomer cements (GICs) have been widely used in dentistry [2]. Due to their excellent biocompatibility in the mouth, with no significant adverse reactions reported in over 20 years of use [3], attention was focused on the development of glass-ionomer bone cement. The past decade has given some impressive advances in the development of medical GICs; however these progresses have been matched by serious critical problems. Firstly, lower mechanical properties of conventional glass-ionomer cement. To overcome this drawback, resin-modified glass-ionomer cements (RMGICs) were developed which combine glass-ionomer chemistry with resin composite technology [4]. Second, there has been detection of aluminum in the brain, cerebral spinal fluid (CSF), urine and blood up to 77 days after surgery [5]. Concerns regarding the release of aluminum from glass-ionomers have led to the development of Fe_2O_3-based conventional glass-ionomer cement by Hurrell-Gillingham et al. [6].

Although the set glass-ionomer cements have several apatite nucleation sites (silanol and carboxyl groups) [7,8], these cements do not show bioactivity after soaking in physiological solutions [9,10] due to the release of polycarboxylic acid. It was shown that even a small quantity (0.1 ppm) of polyacrylic acid (PAA) within the simulated body fluid (SBF) inhibits apatite formation on the surface of apatite–wollastonite glass–ceramic [9]. Furthermore, silica gel which was prepared by hydrolysis and polycondensation of tetraethoxy silane in a water containing polyacrylic acid did not form any apatite layer on its surface [11]. Therefore, it seems difficult to obtain bioactive glass-ionomer cement. However, we previously showed that poorly crystallized hydroxycarbonate apatite layer can be formed on the surface of the new resin-modified glass-ionomer cement [12].

It is well known that the presence of magnetic phases in biomaterials could be used as thermoseed for hyperthermia treatment of cancer [13,14]. Thus, if we could introduce bioactivity in the new resin-modified glass-ionomer cement containing iron oxide, it can be used for wider surgical applications such as treatment of bone tumor and reinforced weakened tumorous bone. In the present study, the change in composition of resin-modified glass-ionomer cement on bioactivity was examined in simulated body fluid.

* Corresponding author. Tel.: +98 2616201887; fax: +98 2616201888.
E-mail address: Jhamak_n@yahoo.com (J. Nourmohammadi).

0272-8842/$36.00
doi:10.1016/j.ceramint.2010.02.031

Table 1
XRF data comparing the chemical composition of the studied glass before and after synthesis.

Oxides	Weight percent (wt.%)	
	Pre-melt glass composition	Post-melt glass composition
SiO_2	22.20	20.80
Fe_2O_3	39.47	33.70
Al_2O_3	–	9.83
P_2O_5	11.68	10.50
CaO	13.81	17.56
CaF_2	12.83	5.66

2. Materials and methods

2.1. Preparation of glass

An ionomer glass composition based on previous studies [6] was synthesized by mixing thoroughly appropriate amounts of reagent-grade chemicals of silica >99.9% pure (Iran, Hamedan), Fe_2O_3 (Merck, 3924, Germany), $CaHPO_4{\cdot}2H_2O$ (Merck, 2146, Germany), $CaCO_3$ (Merck, 2064, Germany) and CaF_2 (Merck, 2840, Germany). The mixture of materials was melted in a covered alumina crucible at 1450 °C for 2 h followed by pouring in cooled water to produce a granular frit. The obtained frit was then ground and sieved to remove particles over 45 μm. The details of the compositions before and after melting were analyzed by X-ray fluorescence spectroscopy (ARL XRF-8410; Table 1). Furthermore, X-ray powder diffraction (XRD; Philips PW 3710) was used to identify the crystal phases present in post-melt glass (Fig. 1).

2.2. Cement preparation

The prepared cement powder and a commercial resin-modified glass-ionomer liquid, Fuji II LC (Improved; batch number 609211, GC Corp., Tokyo, Japan), were mixed at room temperature with a powder to liquid ratio of 2.5 using plastic spatula on a Teflon plate for 40 s. The obtained paste was then placed into the Teflon mould of appropriate dimensions (8 mm × 2 mm), covered with polyethylene strips and held within clamps for 30 s. Afterward, the specimens were exposed to blue light (λ = 400 nm, Farazmehr, Esfahan, Iran) for about 4 min, removed from the mold after 15 min in 100% humidity, and kept in incubator at 37 °C for 24 h prior to testing.

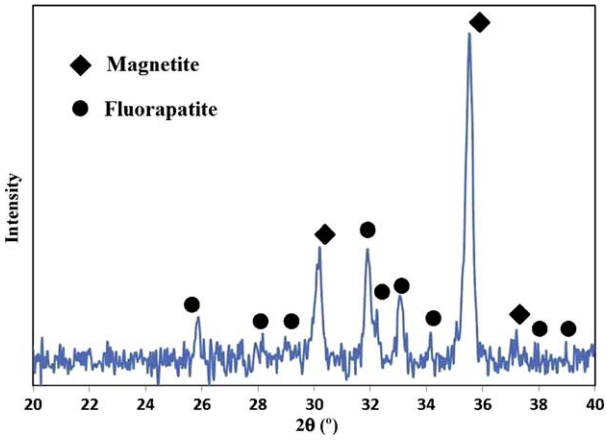

Fig. 1. XRD spectrum of as-casted iron-containing ionomer glass.

2.3. Soaking in simulated body fluid (SBF)

The SBF was prepared by dissolving reagent-grade NaCl (Merck, 6400, Germany), $NaHCO_3$ (Merck, 6323, Germany), KCl (Merck, 4935, Germany), $K_2HPO_4{\cdot}3H_2O$ (Merck, 5099, Germany), $MgCl_2{\cdot}6H_2O$ (Merck, 5833, Germany), Na_2SO_4 (Merck, 13462, Germany), $CaCl_2$ (Merck, 2387, Germany) into de-ionized water, and buffered with Tris (hydroxy-methyl-amino-methane) ($(CH_2OH)_3CNH_2$; Merck, 8387, Germany) and Hydrochloric acid (HCl; Merck, 314, Germany) to pH 7.4 at 37 °C [15]. The concentration of different ionic species in SBF closely resembles that of human blood plasma, as listed in Table 2.

The obtained cements were dipped in polyethylene bottles containing 30 ml of SBF at 37 °C for various periods. The SBF was renewed every 24 h. At the end of the immersion periods, the samples were removed from the SBF, gently cleaned with de-ionized water and dried at room temperature.

2.4. Analysis of solid and solution

The morphologies of the deposits on the surface of the cement were observed by scanning electron microscopy using carbon coating (SEM; CAMBRIGE S360, England), coupled with an energy dispersive spectrometer (EDS). In addition, the features of the cement before and after immersion at different times were studied by atomic force microscopy (AFM). The contact AFM analysis was carried out using a Park CP instrument (Park Scientific Instrument), with constant force mode and silicon nitride tips. The phase composition of the substrate and coating were determined by Philips PW 3710 X-ray diffractometer (CuKα radiation, 40 kV and 30 mA). The 2θ angles ranged from 20° to 40° using 0.01° step and 0/00,058°/s. Furthermore, spectroscopic analysis of pre and post-soaked cement were carried out by the Fourier transform infrared (FTIR; Bruker Vector 33, Germany) using the KBr pellet technique. The dried cement powder before and after immersion (1 mg) was mixed with KBr powder (300 mg) and pressed to form a disk for infrared analysis. The changes in

Table 2
Ion concentration of SBF in comparison with human blood plasma.

Ion species	Ion concentration (mM)	
	SBF solution	Human blood plasma
Na^+	142.0	142.0
K^+	5.0	5.0
Mg^{2+}	1.5	1.5
Ca^{2+}	2.5	2.5
Cl^-	147.8	103.0
HCO_3^-	4.2	27.0
HPO_4^{2-}	1.0	1.0
SO_4^{2-}	0.5	0.5

calcium and phosphorus concentrations in SBF were measured by inductively coupled plasma (ICP; model ARL-3410) and the change of pH values during soaking were determined with a pH meter (ΩMetrohm 827 pH labs, Swiss).

3. Results

XRF analysis of the bulk composition of the glass after synthesis is shown in Table 1. The data indicate the presence of alumina contamination in post-melt glass composition. Moreover, the amount of CaF_2 decreased. However, the measured CaO concentration was higher than in the batch.

Fig. 1 illustrates the XRD pattern of the glass composition before cement formation. The crystal phases in the glass composition were magnetite (Fe_3O_4; JCPDS # 19-629) and fluorapatite ($Ca_5(PO4)_3F$, JCPDS # 15-876) with most important peaks at $d = 2.80$, 2.702 and 2.772.

The XRD patterns of the resin-modified glass-ionomer cement before and after soaking in SBF are shown in Fig. 2. The XRD patterns of the pristine cement show a magnetite phase which was present in the chosen glass powder and hydroxyapatite with major peak at $d = 2.81$, 2.72 and 2.78 (JCPDS standard 84-1998). After 7 days of soaking there was no obvious indication of peaks other than apatite and magnetite. Furthermore, all of the reflection planes showed a clear decrease in their intensity. As time passed the intensity of both phases increased compared to 7 days-soaked cement but they are still less than the base cement. By increasing the immersion time up to 28 days, the amounts of magnetite peaks declined. However, the intensity of apatite peaks increased.

The calcium phosphate formation was monitored by measuring the calcium and phosphorus concentrations as a function of time in SBF. It can be seen from Fig. 3 that a sharp increase and decrease occurred respectively during the early stage of soaking. With time, both ion concentrations raised and then dropped.

As shown in Fig. 4 the initial pH value of SBF (pH = 7.40) decreased quickly to pH = 7.02 in 24 h. Later, an enlargement had been recorded. A decrease followed by an increase comes next.

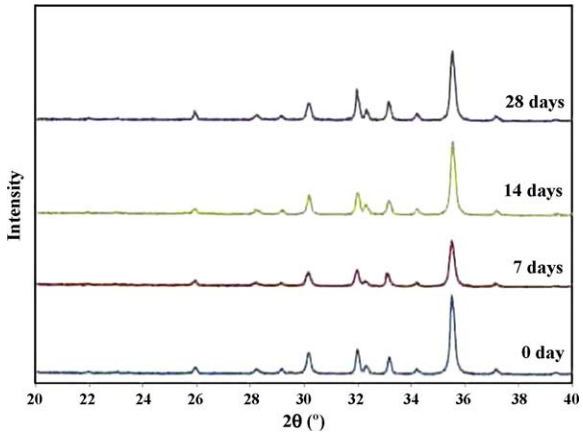

Fig. 2. XRD patterns from the surface of resin-modified glass-ionomer cement before and after soaking in SBF solution.

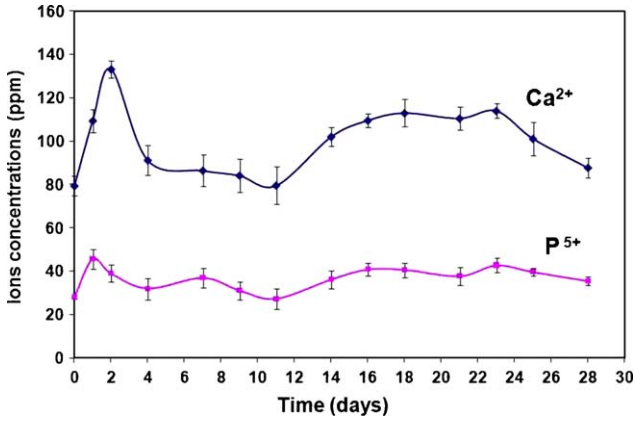

Fig. 3. Change in calcium and phosphorus concentrations of the SBF with soaking time of resin-modified glass-ionomer cement.

Fig. 5 illustrates SEM images of the cement before and after immersion in SBF for different time periods. Glass particles embedded in the polymeric matrix are visible in the base cement before soaking in SBF (Fig. 5a). After 1 day of soaking (Fig. 5b; pH = 7.02), some microcracks were detected on the surface of the cement. However, no precipitations happened in this stage. By increasing immersion time to 48 h (pH = 7.19), some nanometric calcium phosphate deposits were visible on the surface of the cement (Fig. 5c). The SEM image of 7 days-soaked cements (Fig. 5d, pH= 7.65) reveals that some micron size rod-like and nanometric sphere-like calcium phosphate deposits were scattered on the whole surface of the cement. As indicated in Fig. 5e, after 14 days of soaking only rod-like crystals, with crystallites size more than in the 7 days-soaked cement, appeared over the surface. The larger magnification at this stage shows that the underneath surface contains porosities and microcracks similar to the base cement surface (pH = 7.46). For longer immersion time up to 28 days (Fig. 5f), nucleus aggregated in some regions and formed three-dimensional individual clusters such as islands (pH = 7.65). According to the corresponding EDS spectrum of pristine cement (Fig. 5a), the elements detected were mainly calcium, phosphorus, iron, silicon and aluminum. After 28 days of soaking (Fig. 5f) the peaks related to the aluminum were no longer detected and the intensity of the peaks

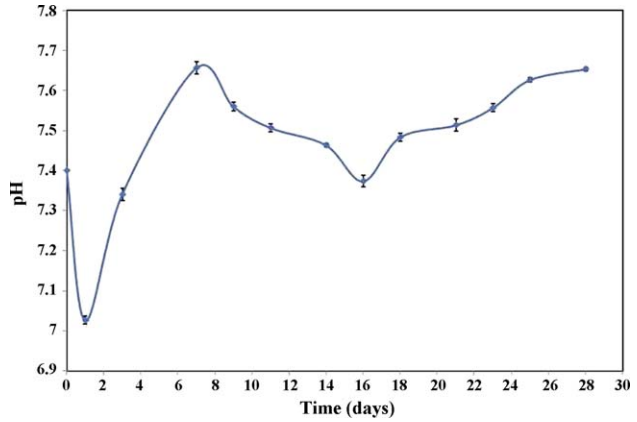

Fig. 4. pH versus time during soaking of the cement in SBF.

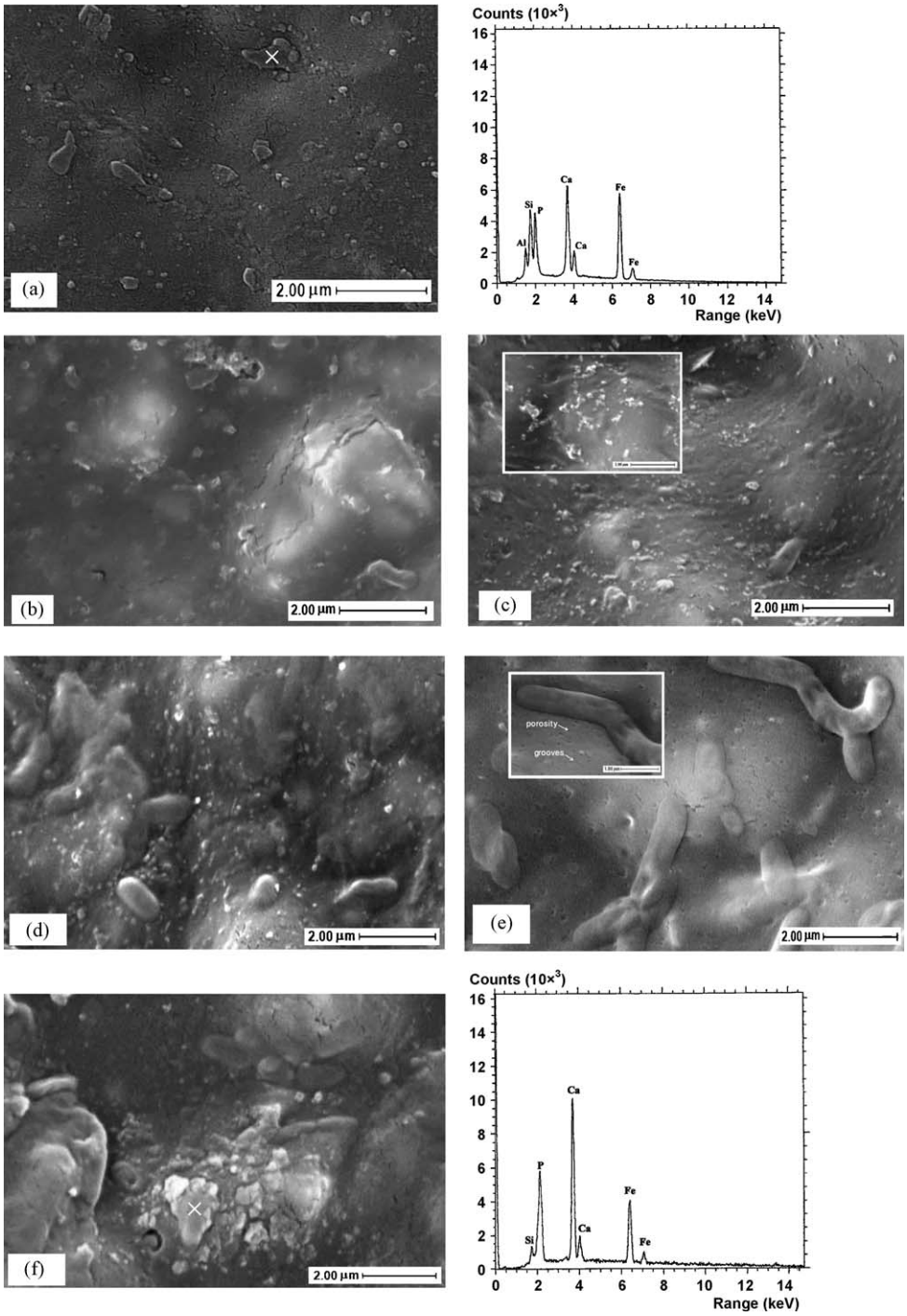

Fig. 5. SEM images and related EDS spectra of resin-modified glass-ionomer cement immersed for different periods (a) 0 day, (b) 24 h, (c) 48 h, (d) 7 days, (e) 14 days and (f) 28 days (magnification = ×10,000, inside pictures ×30,000). In the EDS spectrum of pristine cement calcium, phosphorus, iron, silicon and aluminum were detected. After 28 days of soaking the peaks related to the aluminum were no longer detected and the intensity of the peaks corresponding to silicon and iron decreased and the amount of calcium and phosphorus increased.

corresponding to silicon and iron decreased and the amount of calcium and phosphorus increased.

Fig. 6 shows the topographic profile of the cement surface during soaking in SBF. The AFM image of un-reacted cement shows a porous polymer matrix (Fig. 6a). Soaking in the SBF for 7 days (Fig. 6b) resulted in a change of surface morphology to a smooth one, which suggests that a layer coats the surface of the cement. After 14 days of immersion (Fig. 6c), the cement surface tends to create peak-to-valley structure and elongated nucleates were also observed at this stage. With longer time-spans, three-dimensional clusters similar to the discrete islands appeared on the sample surface (Fig. 6d). The AFM observations corroborated the findings obtained by SEM.

As evident from Fig. 7, the IR spectrum of the cement before soaking shows the peaks at 567 and 600 cm^{-1} due to the υ_4 of PO_4^{3-}, 1050 and 1103 cm^{-1} (υ_3 of PO_4^{3-})[16–18], 1650–

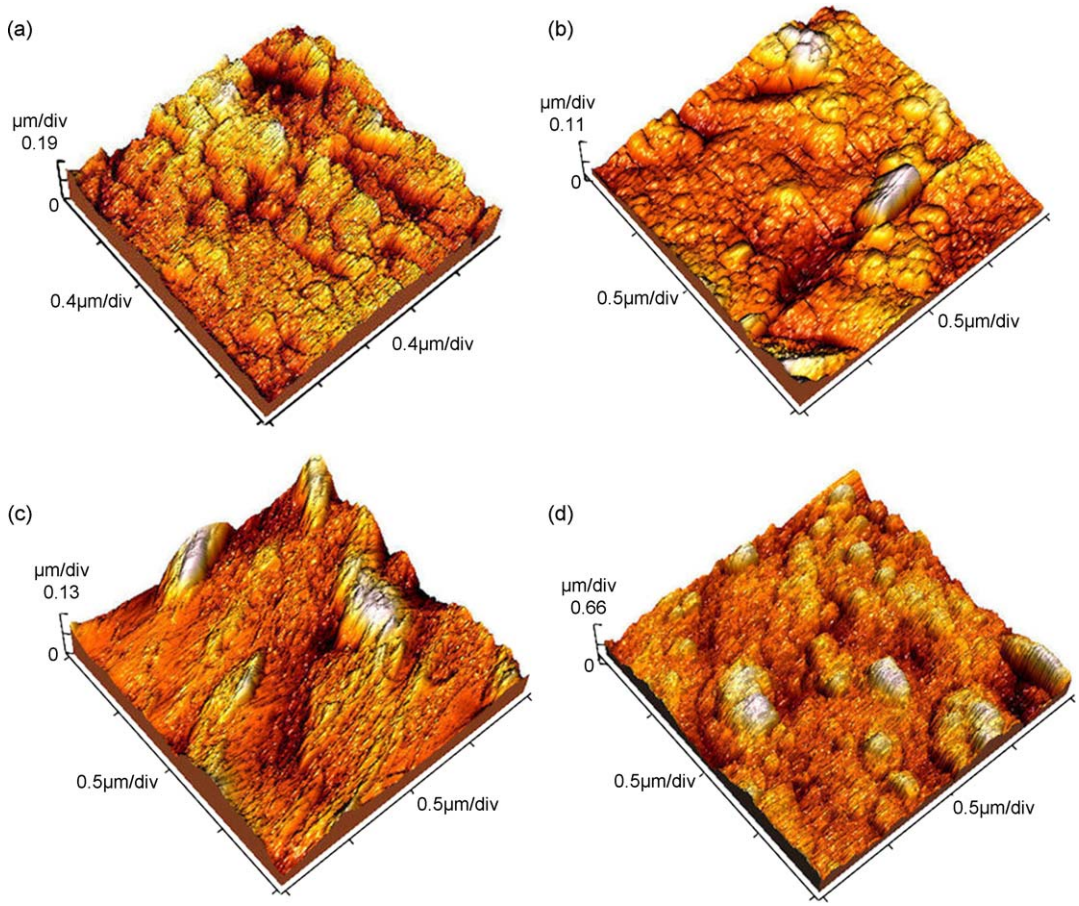

Fig. 6. AFM images of resin-modified glass-ionomer cement immersed for (a) 0 day, (b) 7 days, (c) 14 days and (d) 28 days.

1550 cm^{-1} (asymmetric stretching vibration of COO^- of carboxylic acid salts), 1440–1335 (symmetric stretching vibration of COO^- of carboxylic acid salts) [19] and 1725–1700 cm^{-1} (C=O stretching vibration of ester group of polyHEMA and COOH group in polyacid)[20]. In addition, the absorption bands around the 632 and 3571 cm^{-1} are assigned to the OH stretch and liberation [16–18]. By increasing the immersion time up to 28 days, the FTIR data revealed a number of significant aspects, i.e.:

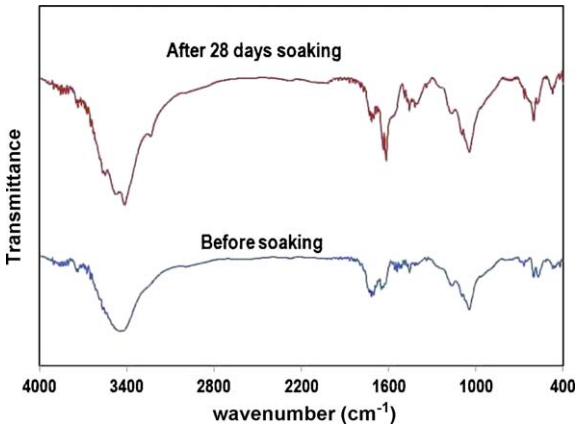

Fig. 7. Change in IR spectra of the experimental cement after 28 days soaking in SBF.

I- The relative intensity of phosphate bands increased.
II- C–O stretching of CO_3^{2-} groups at 1453 and 1413 cm^{-1} is observed.
III- The amount of the C=O and C–O stretching vibration peaks of polyHEMA and polyacids sharply decreased.
IV- The bands in the region of 1650–1530 cm^{-1} enlarged.

4. Discussion

XRF data (Table 1) indicated the presence of small amount of alumina in the glass composition after melting. According to previous reports, ceramic crucibles except alumina crucible were extremely susceptible to Fe_2O_3-based phosphate glasses resulting in complete dissolution of the ceramic crucibles [6]. Furthermore, platinum crucibles are attacked by phosphate containing melt and could not be used for the majority of glasses [6]. So, the chosen glass composition for the present study was melted in alumina crucible due to the least corrosion attack. In addition, compared to the batch composition, the CaF_2 and CaO amounts became respectively lower and higher after melting. This suggests that excessive fluoride loss occurred in the glass composition after melting due to the incorporation of Fe_2O_3 in the ionomer glass composition. It is well known that Al_2O_3 is a main component for maintaining fluoride in ionomer glasses [21].

Despite the presence of fluorapatite in the glass composition (Fig. 1), the formed cement shows the hydroxyapatite phase in its XRD pattern (Fig. 2). This results from the presence of calcium and phosphate ions in the cement powder. As shown in Fig. 7, the characteristic bands in the region 1650–1550 and 1440–1335 cm^{-1} in cured cement before soaking indicate that acid–base reaction also occurred during the setting procedure [20]. Therefore, some of the calcium ions which leached out from the glass during the acid attacks [22], bind with the phosphate groups in the polysalt matrix of the cement which lead to the formation of hydroxyapatite phase in the cement matrix. Moreover, the bands characteristic of phosphate and hydroxyl groups were also detected in the infrared spectrum of the pristine cement (Fig. 7). These peaks confirm the existence of hydroxyapatite in the cement prior to soaking in SBF. It should be mentioned that the occurrence of magnetite in the studied cement indicates that the synthetic cement might be applicable for hyperthermic treatment of bone tumors. It is well established that magnetite (Fe_3O_4) is ferromagnetic and can generate heat by hysteresis loss under an alternate magnetic field [13,14]. After 7 days of soaking (Fig. 2), again the peaks corresponding to the apatite and magnetite were detected on the surface of the cement. However, their intensities decreased at this stage. This implies that an amorphous layer formed on the surface of the 7 days-soaked cement. The enlargement of magnetite peaks after 14 days of soaking (Fig. 2), compared to the 7 days-soaked cement revealed that the most part of the formed layer dissolved. Also, increasing of the calcium and phosphorus amounts (Fig. 3), decreasing of pH (Fig. 4), appearance of microcracks and porosities in SEM (Fig. 5e) and peak-to-valley structure in AFM images (Fig. 6c) during this time period confirm the dissolution process. Furthermore, the increase in the intensity of apatite peaks after 14 days of soaking (Fig. 2) is due to the following reasons: (1) dissolution of the low crystallinity part of the formed layer and (2) growth of rod-like crystals which was supported by SEM images (Fig. 5e). It was found that the intensity of characteristic peaks assigned to apatite became stronger and that of magnetite became weaker after 28 days of soaking. This suggests that the thickness and crystallinity of formed apatite layer on the surface of the cement increased.

SEM images of the 24 h soaked sample shows no apparent coating on the surface (Fig. 5b). Moreover, some microcracks were observed at this time. This result along with decreasing pH values in 24 h (Fig. 4), suggested that extensive release of ions especially acidic ions such as PAA and phosphates occurred during the first day of immersion. A number of evidenced based studies demonstrated that PAA [9,10,23] and Fe^{3+} ions [24,25] are inhibitors for crystallization of apatitic crystals. Interaction between ionized PAA with Ca^{2+} and Fe^{3+} with PO_4^{3-} groups to form intermediate complexes (for example calcium polyacrylate and iron phosphate hydroxide) will hamper apatite formation [26,27]. However, the XRD data in this study indicate no peaks other than apatite and magnetite after 28 days of soaking (Fig. 2).

It is already known that Fe_2O_3 effectively increases the chemical durability of the glasses [24]. Basically the solubility of the chosen glass in the present study is suppressed by Fe_2O_3. Hence, substitution of iron instead of aluminum in current cement decreased the possibility of acid–base setting reaction compared to aluminum containing ionomer cements, which suggested that more calcium ions dissolved from the cement after soaking in the SBF. Therefore, the considerable release of calcium ions from the cement to the SBF (Fig. 3) and the increase of pH (Fig. 4), will dominate the inhibitory effect of polyacrylic acid and iron oxide on apatite formation. In other word, the increment in the concentration of calcium ions in the solution increased the degree of supersaturation (IP/K_0) of SBF with respect to apatite, and consequently enhanced the rate of apatite formation. With time, calcium ions from SBF bind with the negatively charged Si–OH and –COOH groups in the resin-modified glass-ionomer cement (heterogeneous nucleation) and form Ca-rich complexes. Consequently, the complexes incorporated phosphate ions to form apatite nuclei. Once the apatite nuclei are formed on the surface of the studied cement, they grew spontaneously by consuming the calcium and phosphate ions from SBF (Fig. 3).

In agreement with the FTIR spectra of samples (Fig. 7), the appearance of CO_3^{2-} functional groups, increasing the amounts of phosphate and declining the relative intensity of C=O stretching vibration of ester group of polyHEMA and COOH group in polyacid after immersion, pointed to the formation of B-type carbonate apatite layer on the experimental cements. Besides, the enlargements of the peaks in the region 1650–1530 cm^{-1} denoted that some carboxylate salts were formed on the surface of the soaked cement.

As proved by EDS, a calcium phosphate layer formed on the surface of the resin-modified glass-ionomer cement immersed for 28 days in SBF. The SEM and AFM images (Figs. 5f and 6d) of 28 days-soaked sample shows that no continuous and uniform coating was formed except island-like entities on the surface of the cement. Indeed, randomly distributed, three-dimensional nuclei are firstly formed and rapidly approach a saturation density. Afterwards, by growth of these nuclei, observable islands were produced. It seems that the interaction between nucleates are stronger than nucleates with the cement surface, leading to the formation of three-dimensional clusters or islands. This type of growth is known as Volmer–Weber (VW) growth [28].

5. Conclusions

Replacement of iron oxide in ionomer cements will decrease the possibility of acid–base reaction during the setting process of the cement. Consequently, more calcium ions will release from the cement at the initial stage of soaking. The dissolution of calcium ions suppressed the inhibitory effect of polyacrylic acid and iron oxide on apatite formation. Therefore, heterogeneous apatite nucleation occurred on the silanol and carboxyl groups in the cement structure. Eventually, no continuous and uniform coating was formed except island-like entities (Volmer–Weber growth) on the surface of the studied cement. It seems that, the new cured cement would be useful for repairing orthopedic implants to surrounding bone and filling bone defects.

Furthermore, the presence of magnetite phase (Fe_3O_4) in the studied cement demonstrated that the current cement might be a promising material for hyperthermic treatment of cancer.

References

[1] M.A.R. Freeman, G.W. Bradly, P.A. Revell, Observation upon the interface between bone and polymethylmethacrylate cement, J. Bone Joint Surg. B64 (1982) 489.

[2] D.C. Smith, Development of glass-ionomer systems, Biomaterials 19 (1998) 467.

[3] G.J. Mount, Clinical performance of glass-ionomers, Biomaterials 19 (1998) 573.

[4] A.D. Wilson, Resin-modified glass-ionomer cements, Int. J. Prosthodont. 3 (1990) 425.

[5] P.V. Hatton, K. Hurrell-Gillingham, I.M. Brook, Biocompatibility of glass-ionomer bone cements, J. Dent. 34 (2006) 598.

[6] K. Hurrell-Gillingham, I.M. Reaney, I. Brook, P.V. Hatton, In vitro biocompatibility of a novel Fe_2O_3 based glass ionomer cement, J. Dent. 34 (2006) 533.

[7] P. Li, C. Ohtsuki, T. Kokubo, K. Nakanishi, N. Soga, T. Nakamura, T. Yamamuro, Apatite formation induced by silica gel in a simulated body fluid, J. Am. Ceram. Soc. 75 (8) (1992) 2094.

[8] M. Tanahashi, T. Matsuda, Surface functional group dependence on apatite formation on self-assembled monolayers in a simulated body fluid, J. Biomed. Mater. Res. 34 (3) (1997) 305.

[9] M. Kamitakahara, M. Kawashita, T. Kokubo, T. Nakamura, Effect of polyacrylic acid on the apatite formation of bioactive ceramic in a simulated body fluid: fundamental examination of the possibility of obtaining bioactive glass-ionomer cements for orthopaedic use, Biomaterials 22 (2001) 3191.

[10] Z. Amjad, Performance of polymeric additives as hydroxyapatite crystal growth inhibitors, Phosphorus Res. Bull. 5 (1995) 1.

[11] T. Kokubo, Apatite formation on surfaces of ceramics, metals and polymers in body environment, Acta Mater. 46 (7) (1998) 2519.

[12] J. Nourmohammadi, S.K. Sadrnezhaad, A. Behnam Ghader, Bone-like apatite layer formation on the new resin-modified glass-ionomer cement, J. Mater. Sci.: Mater. Med. 19 (2008) 3507.

[13] D.W. Richerson, Modern Ceramic Engineering: Properties, Processing and Use in design, Marcell Dekker, New York, 1992.

[14] M. Kawahita, M. Tanaka, T. Kokubo, Y. Inoue, T. Yao, S. Hamada, T. Shinjo, Preparation of ferromagnetic magnetite microspheres for in situ hyperthermic treatment of cancer, Biomaterials 26 (2005) 2231.

[15] T. Kokubo, H. Kushitani, S. Sakka, T. Kitsugi, T. Yamamuro, Solution able to reproduce in vivo surface-structure changes in bioactive glass–ceramics A-W, J. Biomed. Mater. Res. 24 (1990) 721.

[16] G. Xu, I.A. Aksay, J.T. Groves, Continuous crystalline carbonate apatite thin films: a biomimetic approach, J. Am. Chem. Soc. 123 (10) (2001) 2196.

[17] S.J. Gadaleta, E.P. Paschalis, F. Betts, R. Mendelsohn, A.L. Boskey, Fourier transform infrared spectroscopy of the solution-mediated conversion of amorphous calcium phosphate to hydroxyapatite: new correlations between X-ray diffraction and infrared data, Calcif. Tiss. Int. 58 (1) (1996) 9.

[18] Y. Li, T. Wiliana, K.C. Tam, Synthesis of amorphous calcium phosphate using various types of cyclodextrins, Mater. Res. Bull. 42 (2007) 820.

[19] G. Socrates, Infrared and Raman Characteristic Group Frequencies: Tables and Charts, John Wiley & Sons, Chichester, 2001.

[20] A.M. Young, S.A. Rafeeka, J.A. Howlett, FTIR investigation of monomer polymerisation and polyacid neutralisation kinetics and mechanisms in various aesthetic dental restorative materials, Biomaterials 25 (2004) 823.

[21] K. Hurrell-Gillingham, I.M. Reaney, C.A. Miller, A. Crawford, P.V. Hatton, Devitrification of ionomer glass and its effect on the in vitro biocompatibility of glass-ionomer cements, Biomaterials 24 (2003) 3153.

[22] J. Nourmohammadi, R. Salarian, M. Solati-Hashjin, F. Moztarzadeh, Dissolution behavior and fluoride release from new glass composition used in glass-ionomer cements, Ceram. Int. 33 (2007) 557.

[23] K. Kato, Y. Eika, Y. Ikada, In situ hydroxyapatite crystallization for the hydroxyapatite/polymer composites, J. Mater. Sci. 32 (1997) 5533.

[24] K. Ohura, T. Nakamura, T. Yamamuro, Y. Ebisawa, T. Kokubo, Y. Kotoura, M. Oka, Bioactivity of $CaO{\cdot}SiO_2$ glasses added with various ions, J. Mater. Sci.: Mater. Med. 3 (1992) 95.

[25] K. Singh, D. Bahadur, Characterization of SiO_2–Na_2O–Fe_2O_3–CaO–P_2O_5–B_2O_3 glass ceramics, J. Mater. Sci.: Mater. Med. 10 (1999) 481.

[26] S. Liou, S. Chen, D. Liu, Synthesis and characterization of needle-like apatitic nanocomposite with controlled aspect ratios, Biomaterials 24 (2003) 3981.

[27] L.L. Hench, J. Wilson, An Introduction to Bioceramics, World Scientific, London, 1993.

[28] K.L. Chopra, Thin Film Phenomena, McGraw-Hill, New York, 1969.